Drivers of Change of Thwaites Glacier, West Antarctica, Between 1995 and 2015

Citation for published version:
Santos, TD, Barnes, JM, Goldberg, DN, Gudmundsson, GH & Morlighem, M 2021, 'Drivers of Change of Thwaites Glacier, West Antarctica, Between 1995 and 2015', *Geophysical Research Letters*, vol. 48, no. 20, e2021GL093102. https://doi.org/10.1029/2021GL093102

Digital Object Identifier (DOI):
10.1029/2021GL093102

Link:
Link to publication record in Edinburgh Research Explorer

Document Version:
Peer reviewed version

Published In:
Geophysical Research Letters

Drivers of change of Thwaites Glacier, West Antarctica, between 1995 and 2015

Citation for published version:
Dias Dos Santos, T, Barnes, J, Goldberg, D, Gudmundsson, G & Morlighem, M 2021, 'Drivers of change of Thwaites Glacier, West Antarctica, between 1995 and 2015', *Geophysical Research Letters*, vol. 48, no. 20, e2021GL093102. https://doi.org/10.1029/2021GL093102

Digital Object Identifier (DOI):
10.1029/2021GL093102

Link:
Link to publication record in Edinburgh Research Explorer

Document Version:
Peer reviewed version

Published In:
Geophysical Research Letters

Drivers of change of Thwaites Glacier, West Antarctica, between 1995 and 2015

T. D. dos Santos[1,2,3], J. M. Barnes[4], D. N. Goldberg[5], G. H. Gudmundsson[4], M. Morlighem[6,1]

[1]Escola Politécnica, University of São Paulo, SP, Brazil
[2]Department of Earth System Science, University of California, Irvine, CA 92697, USA
[3]Centro Polar e Climático, Universidade Federal do Rio Grande do Sul, Porto Alegre, RS, Brazil
[4]Department of Geography and Environmental Sciences, Northumbria University, Newcastle upon Tyne, UK
[5]School of GeoSciences, University of Edinburgh, Edinburgh, UK
[6]Department of Earth Sciences, Dartmouth College, Hanover, NH 03755, USA

Key Points:

- The reduction in basal traction due to grounding line retreat plays a critical role on Thwaites dynamics in agreement with previous studies
- Ocean-induced melt leads to a sustained acceleration and grounding line retreat consistent with observations and earlier work
- Improved forecasts of Thwaites demand reliable melt estimates coupled to models that accurately reproduce the response to downstream changes

Corresponding author: T. D. dos Santos, `santos.td@gmail.com`

Abstract

Using three independent ice-flow models and several satellite-based datasets, we assess the importance of correctly capturing ice-shelf breakup, shelf thinning, and reduction in basal traction from ungrounding in reproducing observed speed-up and thinning of Thwaites Glacier between 1995 and 2015. We run several transient numerical simulations applying these three perturbations individually. Our results show that ocean-induced ice-shelf thinning generates most of the observed grounding line retreat, inland speed-up, and mass loss, in agreement with previous work. We improve the agreement with observed inland speed-up and thinning by prescribing changes in ice-shelf geometry and a reduction in basal traction over areas that became ungrounded since 1995, suggesting that shelf breakups and thinning-induced reduction in basal traction play a critical role on Thwaites's dynamics, as pointed out by previous studies. These findings suggest that modeling Thwaites's future requires reliable ocean-induced melt estimates in models that respond accurately to downstream perturbations.

Plain Language Summary

Recent observations have shown that Thwaites Glacier, West Antarctica, has been accelerating and thinning over the past decades and its floating part is quickly breaking up. While these observations suggest that warmer ocean currents are the main factor responsible for these changes, it remains unclear which of the following processes are most important to the glacier's dynamics: (i) breakup of its floating section, (ii) ice-shelf thinning, or (iii) changes in grounded-ice area. By employing three ice-sheet models and several satellite-based datasets, we find that thinning induced by ocean melting and the resulting reduction of grounded-ice area explain most of the observed flow acceleration and mass loss of Thwaites, in agreement with other studies. We also find that the breakup of the floating section plays an important role on Thwaites's dynamics. These findings suggest that improved forecasts of Thwaites's future require reliable ocean-induced melt estimates and improved model response to changes in ice-shelf thickness and geometry.

1 Introduction

Thwaites Glacier, one of the largest ice streams in the Amundsen Sea Embayment (Fig. 1), drains a large area of the West Antarctic Ice Sheet (WAIS). Its ice volume holds the equivalent of $\sim$0.65 m of sea level (Morlighem et al., 2020), and is resting on deep bedrock, a wide channel below sea level that spreads under WAIS to the Ross Sea Embayment (Holt et al., 2006; Fretwell et al., 2013). The retrograde slope of this channel makes Thwaites potentially vulnerable to marine ice sheet instability (Weertman, 1974; Schoof, 2007; Gudmundsson et al., 2012), a positive feedback of grounding line retreat and increased ice discharge, which may lead ultimately to WAIS's collapse over the coming centuries (Bamber et al., 2009; Joughin et al., 2014; Feldmann & Levermann, 2015; Scambos et al., 2017; Martin et al., 2019). How fast this collapse may happen depends on internal instability mechanisms (e.g., Favier et al., 2014) and on external forcings that could drive significant mass loss of Thwaites Glacier and WAIS (e.g., Gudmundsson et al., 2019).

Recent observations have shown that Thwaites has been accelerating, thinning and experiencing ice-shelf breakups and grounding line retreat since the 1970s (Mouginot et al., 2014; Rignot et al., 2014; Konrad et al., 2018; Shepherd et al., 2019). The pattern of ice thinning in the Amundsen Sea Sector suggests that changes in ocean conditions are likely the main external driver of ocean-induced ice-shelf thinning, increased calving rates, and changes in grounding line positions (Alley et al., 2015; Seroussi et al., 2017; Milillo et al., 2019). Although these changes are not independent, the exact chain of events that led to Thwaites's thinning and acceleration remains unclear. For instance, the increased thinning of the ice shelves may have compromised their mechanical integrity, lead-

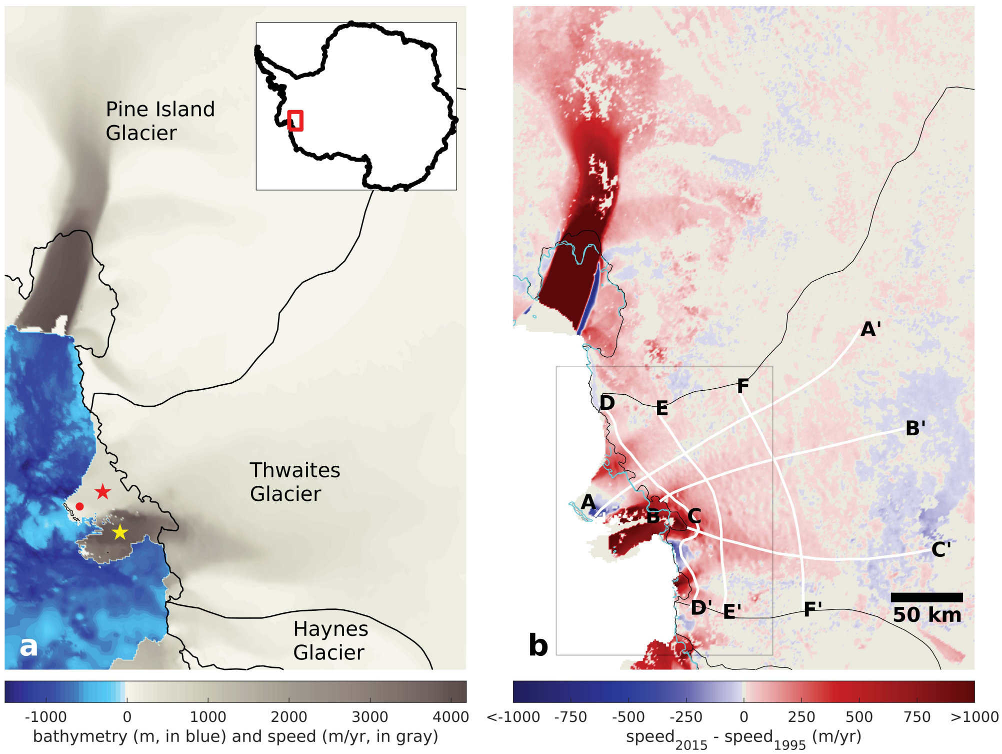

Figure 1. (a) Ocean bathymetry (blue scale in colorbar) and ice speeds (gray scale), and (b) observed speed changes between 1995 and 2015 (Mouginot et al., 2014) of the two largest ice streams of the Amundsen Sea Sector, West Antarctica: Pine Island and Thwaites glaciers. In (a), the red star shows the location of Thwaites Eastern Ice Shelf (TEIS) and the yellow star shows Thwaites Tongue (TT). The red circle shows the location of the pinning point at TEIS's tip. The black lines delineate the drainage basin and the 2015 grounding lines. In (b), the white lines show flow lines and cross sections used in this paper. Transect A-A' is referred to as eastern ice stream, transect B-B' as the main trunk, and transect C-C' as the western ice stream. Lines in light blue are the 1995 grounding line. The box highlights the area shown in Fig. 2.

ing to the partial collapse of Thwaites Eastern Ice Shelf (TEIS) and the complete loss of Thwaites Tongue (TT) (e.g., Scambos et al., 2009; Miles et al., 2020). These changes could have decreased the buttressing provided by the pinning point in TEIS's tip to the grounded ice (Fig. 1, panel a), inducing glacier speed-up and, as a consequence, the retreat of the grounding line (Fig. 1, panel b).

We investigate the effect of each of these physical processes on numerical modeling of Thwaites's dynamics between 1995 and 2015. We perform several numerical simulations using three independent ice sheet models (Úa, ISSM, and STREAMICE) for which we prescribe changes in calving front position, ice-shelf thickness, and basal traction due to grounding line retreat, and we quantify their impacts on upstream flow. The resulting changes in ice speed and thickness are compared with satellite-based measurements. The misfit between modeled and observed ice velocities in each case provides estimates of the relative importance of all those observed changes on the glacier flow.

2 Data and Methods

2.1 Data

The three models are initialized to 1995 conditions and are run forward in time until 2015. The 1995 digital elevation model (DEM) is derived from the European Remote Sensing (ERS-1) radar altimetry (Bamber, 2000). The 2015 DEM is the Reference Elevation Model of Antarctica, REMA (Howat et al., 2019), included in BedMachine Antarctica v2 (Morlighem et al., 2020). We employ the most recent bed elevation product derived from mass conservation and recent survey in Thwaites (Hogan et al., 2020; Jordan et al., 2020; Morlighem et al., 2020). Ice velocities and grounding line positions of the initial (1995) and final (2015) states are derived from interferometric synthetic aperture radar data (InSAR, Mouginot et al., 2014; Rignot et al., 2014).

As described in Sect. 2.3, we impose perturbations based on satellite measurements. Changes in calving-front extension are derived from Landsat imagery (MacGregor et al., 2012). Ice-shelf thinning rates are estimated by radar altimetry (Paolo et al., 2015). Grounding line retreat is measured by InSAR data (Rignot et al., 2014). We compare the modeled velocity change and thinning rates with observations of speed change and ice thinning derived from InSAR and radar/laser altimetry data, respectively (Mouginot et al., 2014; Shepherd et al., 2019; Smith et al., 2020). The basal melting is parameterized by a depth-dependent relationship based on observations and ice-ocean-coupling simulations (Rignot et al., 2013; Seroussi et al., 2017; Milillo et al., 2019; Nakayama et al., 2019). The surface mass balance is derived from the Regional Climate Model (RACMO v2.3, Van Wessem et al., 2014).

Landsat imagery shows a rift propagating between TEIS and TT from the 1980s to 2010/2011, when the main part of TT calved off (MacGregor et al., 2012). Based on the hypothesis of a non-negligible shear stress between TEIS and TT prior to 2006 (Mouginot et al., 2014; Miles et al., 2020), likely due to mélange formation that could act as a granular ice shelf (Burton et al., 2018) into that rifted zone, we start all the experiments in 1995 with TEIS and TT mechanically connected. To set up this connection, we remove this rift from the 1995 Landsat-derived ice-front contour, allowing transfer of stresses across the region where the rift later developed. The model initialization (inversion, see Sect. 2.2) adjusts the rheological parameter of the ice into that rifted zone to model the speed differences between TEIS and TT (Fig. 1, panel a). We keep the 1995 shelf-front position fixed in time, except where otherwise stated (see Sect. 2.3).

2.2 Ice sheet models

To assess the robustness of our conclusions with respect to the use of ice sheet models and ice-flow assumptions, we employ three ice sheet models: Úa (Gudmundsson, 2020), ISSM (Larour et al., 2012), and STREAMICE (Goldberg & Heimbach, 2013). Úa employs the two-dimensional Shallow Shelf Approximation (SSA; MacAyeal, 1989), ISSM a three-dimensional High-Order model (HO; Blatter, 1995), and STREAMICE a two-dimensional L1L2-type approximation (Goldberg, 2011; Lipscomb et al., 2019).

The model domains comprise the Amundsen Sea Embayment catchment, including Pine Island, Thwaites, and neighboring glaciers (Haynes, Pope, Smith, and Kohler glaciers). The model domains and meshes are similar to those in Barnes et al. (2021). ISSM and Úa's meshes rely on Delaunay triangulation with edge lengths varying according to an interpolation error estimate of the observed ice velocity and on the distance to the grounding line. In ISSM, a 500 m mesh resolution is employed close to the grounding line and 15 km on the far field. ISSM generates the three-dimensional mesh by extruding the two-dimensional triangular mesh. In Úa, 1 km resolution is used near the grounding line, while a coarser resolution (up to 20 km) is used inland. STREAMICE relies on a quadrilateral-element-type mesh with uniform element's edge length equal to 1.5 km. These resolutions are sufficient for this type of experiment (e.g., Cornford et al., 2020).

All models employ a Weertman's sliding law (Weertman, 1957):

$$\boldsymbol{\tau}_b = -\beta^2 \|\boldsymbol{v}_b\|^{\frac{1}{m}-1}\, \boldsymbol{v}_b \tag{1}$$

where $\boldsymbol{\tau}_b$ is the basal drag (the bed-parallel component of the bed traction), β^2 is the drag coefficient, $\boldsymbol{v}_b$ is the basal velocity, and we here assume the commonly-used value of $m = 3$. We note that the impact of the stress exponent m on modelled changes in ice flow have been studied previously in a number of studies, e.g. a recent study on the drivers of change over Pine Island Glacier by De Rydt et al. (2021).

Each model performs its own inversion procedure to infer the spatial distributions of the basal drag coefficient β^2, and an ice rheological parameter, commonly denoted as A, in Glen's flow law, using 1995 data (DEM and ice velocity; Bamber, 2000; Mouginot et al., 2014) and ice temperatures calculated by other studies (Seroussi et al., 2019; Van Liefferinge & Pattyn, 2013). All three models invert for β^2 over grounded ice. Úa and STREAMICE invert for the ice rheological parameter A over the entire domain (with STREAMICE penalizing variations from a 'prior' temperature-based estimate in grounded ice), while ISSM inverts for A only on floating ice. Technical details of the model inversions are described in Barnes et al. (2021). The resulting spatial distributions, i.e., $\beta^2(x, y)$ and $A(x, y)$, are kept constant over the transient runs (except for the experiments where we manually decrease β^2 in specific areas, Sect. 2.3).

The models set the basal traction to a negligible value downstream of the 1995 grounding-line position, which helps to prevent the grounding line from advancing beyond its initial state. The grounding line is based on hydrostatic equilibrium (Seroussi et al., 2014) and is free to migrate in all experiments.

2.3 Numerical experiments

2.3.1 Control experiment

We first run a 'control' simulation forced by ice-shelf melting only. None of the observed changes in geometry are imposed during the transient runs, and the ice-shelf thickness and the position of the grounding line are therefore free to evolve in response to this ice-shelf melting. Note that in this control simulation the models may not necessarily reproduce the observed ice-shelf thinning and grounding line retreat since those are unconstrained in this experimental setup.

Basal melting under floating ice, m_b (in m/yr, positive if melting), is described by a depth-dependent function (see Fig. S1 and S2 in Seroussi et al., 2017):

$$m_b = \begin{cases} 50/500\,|z_b|, & \text{if } 0 \geq z_b > -500\,\text{m}, \\ 50, & \text{if } z_b \leq -500\,\text{m}, \end{cases} \tag{2}$$

where z_b (in m) is the ice-shelf base depth (negative if below sea level).

We apply melt only to elements/cells containing fully floating ice (Seroussi & Morlighem, 2018). The parameters in Eq. 2 are kept fixed during the simulations, although the spatial distribution of basal melting varies in time with the evolving thickness and extent (due to grounding line migration) of the ice shelf.

2.3.2 Imposed change experiments overview

Since the grounding line and ice-shelf thickness evolve freely in the control experiments, we expect that the agreement with observed speed and thickness change will be improved if we constrain front geometry, ice-shelf thinning, and loss of basal drag in the models, all according to observed changes. Prescribing these changes individually allows their respective impacts on the modeled evolution to be quantified and compared. For example, if applying the observed change in ice-front position improves the agreement with observations, it would suggest that calving dynamics played a role in the behavior of Thwaites. Comparing the response of the models will also shed light on the processes that have the strongest effect on Thwaites's dynamics.

We run simulations where we apply observed changes to the control setup in (i) ice-front position, (ii) ice-shelf thickness, and (iii) basal traction downstream of the 2015 grounding line, all based on observations. We force the models to follow these changes individually by prescribing these observed changes directly in the models. We also run (iv) an all-external-drivers experiment, where (i), (ii), (iii), and melt are all applied. We expect the results of experiment (iv) to be more consistent with observations. All experiments employ basal melt as given by Eq. 2, unless otherwise specified.

2.3.3 Ice-front change experiment

The observed retreat and rift propagation on Thwaites's floating ice are imposed on a yearly basis at the ice-ocean boundary, following Landsat imagery (MacGregor et al., 2012). Any dynamic effect from ice-shelf rifting or collapse is captured in this simulation. We apply these changes only to regions downstream of the 1995 grounding-line position. We keep TEIS and TT mechanically connected until 2005, following the hypothesis mentioned in Sect. 2.1. To this end, we remove the rift between TEIS and TT from the Landsat-derived ice-front contours for all years between 1996 and 2005. From 2006 to 2015, we impose the original Landsat-based contours, disconnecting TEIS and TT (MacGregor et al., 2012). We do not consider any healing of that link after 2006 (Mouginot et al., 2014; Miles et al., 2020), since TT calved off in 2010/2011 (MacGregor et al., 2012). The basal melt is applied to all floating ice.

2.3.4 Ice-shelf thinning experiment

The 1995 shelf thickness is manually decreased according to satellite-measured thinning rates (e.g., Paolo et al., 2015; Smith et al., 2020). The 1995 shelf thickness is proportionally changed at each time step from 1995 to 2015. This setup simulates the effect of decreasing ice-shelf buttressing on grounded ice following the observed shelf thinning. The imposed thinning 'overrides' melting except in newly ungrounded ice where the thinning is not applied, i.e., the melt is only applied to areas upstream of the 1995 grounding line that become ungrounded during the transient runs. Imposing the thinning manually recovers the observed shelf-thickness change, which would probably not be perfectly reproduced by our parameterized basal melt in the control experiment (see Fig. S3 and S6).

2.3.5 Loss of basal traction experiment

Due to the lack of spatial and temporal data availability and the technical challenge of preserving hydrostatic equilibrium at the grounding line, we cannot directly prescribe the grounding line positions in transient runs. Instead, we simulate the effect of observed grounded ice retreat by linearly decreasing β^2 with time from its 1995-inverted value to zero between 1995 and 2015. The value of the basal drag coefficient, β^2, is reduced only in the region that was grounded in 1995 but floating in 2015 (Rignot et al., 2014). This setup simulates a thinning-induced reduction in basal traction: as the ice approaches flotation, the effective pressure declines, reducing the basal traction. Note that the control experiment would not necessarily be reproducing this physical process and the observed grounding line retreat. The basal melt applies to all floating ice.

2.3.6 All-external-drivers experiment

The setup imposes the three observed changes together. These changes are the same as those imposed in the experiments described in Sects. 2.3.3, 2.3.4, 2.3.5. The melt is applied only to areas upstream of the 1995 grounding line that become floating over the simulations.

3 Results

To assess the relative impact of each imposed change on the models, we compute correlations and root mean square errors (RMSE) between observed and modeled speed and thickness change. The correlations measure the agreement between spatial patterns, while the RMSE quantifies the magnitude of the misfits.

3.1 Ice velocity changes

The observed acceleration of Thwaites Glacier has not been spatially uniform (Mouginot et al., 2014). The ice velocity increased by up to 25 m/yr per year in the vicinity of the grounding line (Fig. 1, panel b). Most of the main trunk and the western ice stream have been accelerating markedly up to 100 km upstream of the glacier's margin. The eastern part of the glacier has not changed significantly, except around the eastern margin of TEIS (see L1 in Fig. 2, panel a1) which accelerated by up to 20 m/yr per year. Most of the regions that sped up coincide with the regions where the grounding line retreated during this period (Fig. 1, panel b). Only a small area at the terminus of the western ice stream (see L2, Fig. 2, panel a1) decelerated between 1995 and 2015. At this location, the grounding line has not changed since the 1990s. The ice flux at the 2011 grounding line of Thwaites increased 30-33±5 Gt/yr over the 1994/1996-2013 period (Mouginot et al., 2014) (see Table S2).

The control experiment produces grounding line retreat and inland speed-up with moderate correlations in comparison to other experiments (Fig. 2, panels b1, b2, and b3, and Table 1). The modeled increase in ice flux is also comparable to observations and varies from 20 Gt/yr (ISSM) to 30 Gt/yr (STREAMICE) (Table S2).

Applying observed changes individually produces some differences among the model responses, with some simulations producing substantially better improvements in misfit and correlation for some models (e.g., ice-front change for Úa and ice-shelf thinning

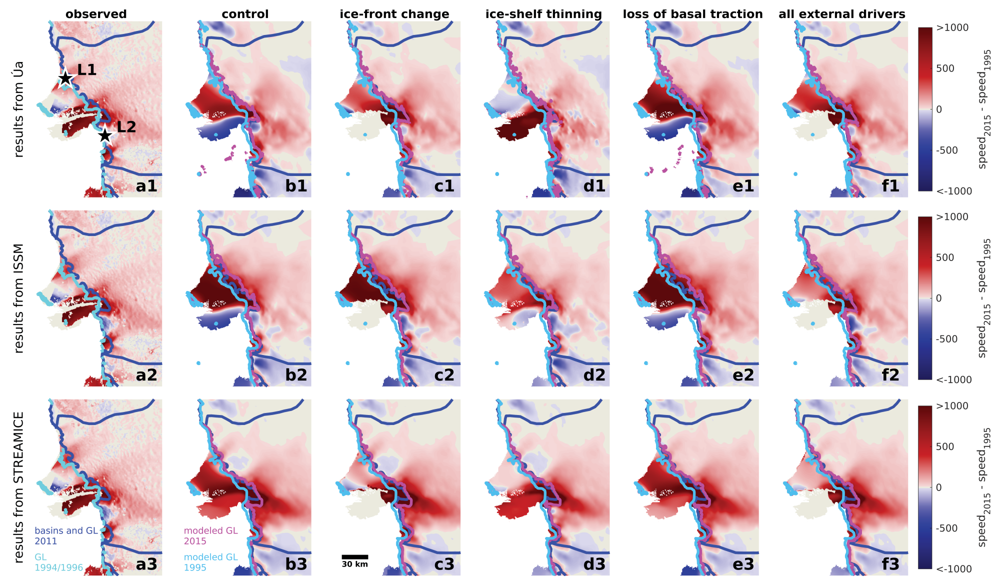

Figure 2. Speed changes of Thwaites Glacier obtained by the transient numerical experiments described in Sect. 2.3. The speed changes are obtained by subtracting the initial speed (1995) from the final speed (2015). Three ice sheet models are used: (b1-f1) Úa, (b2-f2) ISSM, and (b3-f3) STREAMICE. (a1-a3) observed speed change (panels a1, a2, and a3 show the same map, for comparison purposes). (b1-b3) control experiment. (c1-c3) ice-front change experiment. (d1-d3) ice-shelf thinning experiment. (e1-e3) loss of basal traction experiment. (f1-f3) all-external-drivers experiment. The panels show the initial and final grounding line positions (from InSAR data and from the models, see the legends portrayed on panels a3 and b3, respectively). In (a1), black stars highlight two regions of localized speed changes (L1 and L2). Location 1 (L1) indicates the acceleration of the eastern margin of TEIS, and location 2 (L2) indicates a region that decelerated in the margin of the western ice stream.

Table 1. Correlations and root mean square errors (RMSE) between modeled and observed speed and thickness changes obtained by the experiments described in Sect. 2.3. The correlations and RMSE for thickness change are calculated using two different data sets: (a) from Shepherd et al. (2019), whose time period is 1992-2017, and (b) from Smith et al. (2020), whose time period is 2003-2019. We apply a Gaussian filter to the modeled thickness changes with kernel size equal to 35 km and $\sigma = 0.20$, following Smith et al. (2020). All correlation coefficients and RMSE are obtained considering Thwaites's basin and inland extension as given by transect A-A' portrayed on panel b of Fig. 1. Legend: CR (control experiment), IF (ice-front change experiment), IS (ice-shelf thinning experiment), BT (loss of basal traction experiment), and AD (all-external-drivers experiment).

	CR	IF	IS	BT	AD	CR	IF	IS	BT	AD
Speed change	Correlation					RMSE (m/yr)				
Úa	0.58	0.74	0.55	0.67	0.77	17.53	10.47	17.39	17.14	10.29
ISSM	0.58	0.69	0.61	0.69	0.74	14.46	14.17	12.19	15.35	10.37
STREAMICE	0.70	0.72	0.76	0.72	0.73	25.36	26.98	18.91	24.72	24.08
Thickness change (a)	Correlation					RMSE (m)				
Úa	0.79	0.85	0.71	0.84	0.88	4.20	4.50	4.33	4.53	4.81
ISSM	0.84	0.86	0.81	0.90	0.89	5.47	5.95	3.83	6.72	5.00
STREAMICE	0.82	0.81	0.80	0.86	0.84	6.67	7.81	6.69	7.49	7.94
Thickness change (b)	Correlation					RMSE (m)				
Úa	0.78	0.87	0.71	0.83	0.89	4.86	3.53	5.69	4.55	3.48
ISSM	0.79	0.82	0.80	0.86	0.88	4.71	4.80	3.75	5.10	3.55
STREAMICE	0.86	0.86	0.85	0.89	0.88	4.53	5.53	4.59	5.10	5.52

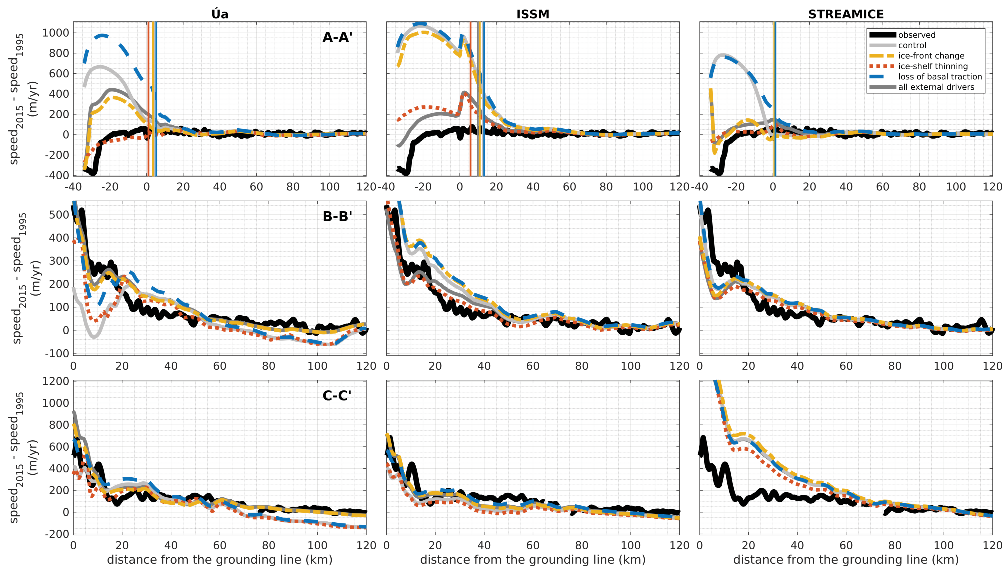

Figure 3. Speed changes at the end of the transient experiments (2015) over flow lines: A-A', B-B', and C-C'. The experiments are described in Sect. 2.3. The InSAR-derived speed change is in black. The distance from the grounding line refers to the 2015-observed grounding line position. Vertical lines shown on transect A-A' panels are the grounding line positions at the end of the experiments (2015). All flow lines' locations are shown in Fig. 1.

for STREAMICE) than for others. In Úa, prescribing ice-shelf thinning appears to introduce numerical inconsistencies at the boundary of the area for which thickness is enforced, which explains the differences in the shape of the grounding line compared to other experiments (Fig. 2, panel d1).

As expected, the all-external-drivers experiment reproduces the overall pattern of observed speed change with the least error, including the localized changes at L1 and L2 (Fig. 2, panels f1, f2, and f3). Changes in L2 are not captured by STREAMICE because the grounding line retreats in this region with this model. Overall, the final modeled grounding line positions obtained with the all-external-drivers experiment are also in good agreement with observations. STREAMICE overestimates grounding line retreat along the western side of the grounding line 'bight' in front of western Thwaites (location 'A' of Milillo et al., 2019). This overestimated retreat coincides with overestimated acceleration in the western part of Thwaites (Fig. 2, panels from b3 to f3, and Fig. 3, transect C-C'), which contributes to the higher RMSE and glacier flux compared to Úa and ISSM (Tables 1 and S2, respectively). The increase in glacier flux varies from 15 Gt/yr (ISSM) to 30 Gt/yr (STREAMICE) (Table S2).

3.2 Ice thinning

The observed thinning of Thwaites followed the observed ice speed-up, extending tens of kilometers over the interior of the glacier (Fig. S9, panel a1). The margins of the main trunk and western ice streams as well as the eastern part of TEIS (L1) thinned the most (up to 45 m over the 2003-2019 period; Smith et al., 2020). To compare with our results, we use two different datasets of observed thickness changes (Shepherd et al., 2019; Smith et al., 2020), since they employ an acquisition period different from the period considered here (see Table 1).

The three ice sheet models produce patterns of ice thinning similar to observations in all experiments, as seen by the relatively high correlations (Table 1), although some thickening appears in regions around the glacier's basin likely due to thickness adjustments during the transient runs. The inland thickening produced by Úa in the ice-shelf experiment is likely caused by the numerical inconsistencies described above.

The control experiment generates a pattern of thickness change comparable to observations, as noted by the relatively high correlation of ∼0.81. The thinning rates obtained with all-external-drivers and loss of basal traction experiments show the highest correlation coefficients (∼0.88 and ∼0.86, respectively), followed by ice-front change (∼0.85) and ice-shelf thinning (∼0.78) experiments.

4 Discussion

The control experiment produces upstream acceleration, thinning, and grounding line migration comparable to observations. Our parameterized melt is not necessarily in balance with the ice-shelf flow (e.g., Rignot et al., 2013), which produces some shelf thinning (Fig. S6). As a consequence, the melt sustains thinning of newly-ungrounded ice upstream of the 1995 grounding line as downstream changes (i.e., shelf thinning) induce a loss of buttressing on upstream flow (e.g., in the vicinity of the grounding line along the main trunk and the western ice stream), causing inland speed-up, thinning, and grounding line retreat. This mechanism may be enhanced by local reverse-slope bedrock, where the grounding line may retreat faster (Schoof, 2007; Joughin et al., 2014; Rignot et al., 2014; Seroussi et al., 2017; Morlighem et al., 2020). The observed mass loss over the last decades in the Amundsen Sea Sector is therefore likely associated with increasing ocean-induced melt (e.g., Pritchard et al., 2012; Joughin et al., 2014; Jenkins et al., 2016; Seroussi et al., 2017; Martin et al., 2019; Milillo et al., 2019; Hoffman et al., 2019; Robel et al., 2019).

In the experiments where we impose observed changes instead of letting the model evolve freely, we find that forcing the geometry of the ice shelf and basal traction increases the correlations in both speed change and ice thinning. These findings suggest that rifting propagation between TEIS and TT and thinning-induced reduction in basal traction play an important role on Thwaites's dynamics, as pointed out by previous studies (e.g., Mouginot et al., 2014; Miles et al., 2020; Joughin et al., 2014; Nias et al., 2016). Given its importance, the evolution of basal drag as the grounding line retreats may therefore need to be further improved in ice-sheet models (Nias et al., 2016; De Rydt et al., 2021). For instance, we employ here Weertman's sliding law with an exponent $m = 3$ and we invert for the drag coefficient (β^2). The resulting spatial distribution of β^2 is then kept fixed in all simulations (except for the loss of basal traction setup). Other sliding laws that reduce the basal traction as the grounding line migrates could potentially generate a different upstream response to ice thinning/front retreat (Brondex et al., 2017, 2019; Joughin et al., 2019; De Rydt et al., 2021). Also, it remains unclear whether a 'mechanical link' between TEIS and TT could be reinstated in the future, or whether the mechanical integrity of TEIS will be compromised due to structural weakening (e.g., Miles et al., 2020). Thus, enhanced calving dynamics may also improve the accuracy of numerical simulations of Thwaites (e.g., Crawford et al., 2021).

Our parameterized basal melt is based on observations and ocean simulations, and similar parameterizations have been used in other studies of Thwaites Glacier (Depoorter et al., 2013; Rignot et al., 2013; Milillo et al., 2019; Seroussi et al., 2017; Nakayama et al., 2018, 2019; Joughin et al., 2014; Hoffman et al., 2019). At the end of the control experiments, the integrated melt is, on average, 110 Gt/yr, which is slightly greater than satellite-based (97.5±7 Gt/yr, Rignot et al., 2013) and simulation-based (80-120 Gt/yr, Seroussi et al., 2017) estimates (see Table S1 and Fig. S10). Depth-dependent melt parameterizations tend to overestimate grounding line retreat in comparison to ice-ocean simulations in longer runs (Seroussi et al., 2017). The parameters in Eq. 2 were kept constant over the transient runs, although it is likely that ocean conditions have changed over the last decades, which could have affected the response of the models. For instance, rerunning the control experiment in ISSM with the parameterized melt multiplied by 4, the model overestimates the inland acceleration (the resulting RMSE is 28.58 m/yr. See also Fig. S5, panel b) and the integrated melt along the entire transient run (Fig. S10), although the spatial pattern of the response is similar to observations (correlation of 0.78). To improve the forecast of Thwaites's future, reliable estimates of melt rates are required, especially close to the grounding line, where thinning-induced reduction in basal traction is critical.

The differences between the models' results may be caused by several factors: stress balance approximation, inversion procedure, mesh resolution, numerical issues caused by imposed forcings, etc. (e.g., Cornford et al., 2020; Barnes et al., 2021). STREAMICE had more extensive retreat in the western part of the Thwaites grounding line than that of Úa or ISSM, which might be the reason for larger acceleration in this region and resulting higher RMSE. The difference may arise from a differing treatment of a small ice rise in TT arising from a topographic high in the bathymetry data (see the supporting information), or from resolution in the vicinity of the grounding line which may be too coarse (Cornford et al., 2020). A deceleration can be seen upstream in some Úa results, particularly evident across transect F-F' in Fig. S8, due to slight differences in the inverted basal sliding and rate factor fields compared to the other models. These factors all play an important role in transient simulations and shall be investigated in future work. Our results also illustrate how challenging reproducibility is in the field of ice sheet modeling (e.g., Seroussi et al., 2020), which calls for further numerical developments and model inter-comparison initiatives.

Uncertainties in the data and inversion procedures may have an impact on our results. For example, the mass loss observed from over the last decades could be part of an already existing dynamic imbalance prior to 1995, and our inversions were not able to capture this early loss trend. Also, using a previous bed elevation version (BedMachine v1), artificial 'bumps' downstream of the 2015 grounding line (and close to the 1995 grounding line) prevented inland acceleration and grounding line retreat in most of the experiments. These results highlight the need for further improvements in bed topography data, as noted by others (e.g., Durand et al., 2011; Nias et al., 2016).

5 Conclusions

By conducting time-dependent numerical simulations of Thwaites Glacier between 1995 and 2015 with three independent ice sheet models and several satellite-based datasets, we find that thinning induced by ocean melting and the resulting grounding line retreat explain much of the observed speed-up of Thwaites. The models also suggest that changes in the ice-shelf geometry, especially the rifting propagation between the Eastern Ice Shelf and Thwaites Tongue, improve the agreement with observations. The results suggest that improved forecasts of Thwaites's future require reliable ocean-induced melt estimates and improved model response to downstream perturbations, particularly thinning-induced reduction in basal traction.

Acknowledgments

This work is from the PROPHET project, a component of the International Thwaites Glacier Collaboration (ITGC). Support from National Science Foundation (NSF: Grant #1739031) and Natural Environment Research Council (NERC: Grants NE/S006745/1 and NE/S006796/1). ITGC Contribution No. ITGC-023. All of the data sets and source codes used in this study are publicly available. The Ice-sheet and Sea-level System Model can be accessed at `https://issm.jpl.nasa.gov` (we used version 4.18). STREAMICE

is a module of MITgcm and can be download at `https://mitgcm.org/source-code/`. The source code of Úa can be downloaded at `http://doi.org/10.5281/zenodo.3706623`. BedMachine Antarctica is available at NSIDC (`http://nsidc.org/data/nsidc-0756`). The 1995 Antarctic 5 km DEM is also available at NSIDC (`https://nsidc.org/data/nsidc-0076`). InSAR-Based ice velocity of the Amundsen Sea Embayment is found at NSIDC (`https://nsidc.org/data/NSIDC-0545`). Coastal and terminus history of Thwaites (shapefile format) is found at NSIDC (`https://nsidc.org/data/NSIDC-0522`). Grounding line positions are found at NSIDC (`https://nsidc.org/data/NSIDC-0498`). Maps of thickness changes are found at Nasa's EarthData (`https://sealevel.nasa.gov/data/dataset/?identifier=SLCP_ice_shelf_dh_v1_1`), University of Washington's digital repository (`https://digital.lib.washington.edu/researchworks/handle/1773/45388`), and at CPOM (`http://www.cpom.ucl.ac.uk/csopr`). The Antarctic surface mass balance (RACMO 2.3) is available at `https://www.projects.science.uu.nl/iceclimate/models/antarctica.php`.

References

Alley, R. B., Anandakrishnan, S., Christianson, K., Horgan, H. J., Muto, A., Parizek, B. R., ... Walker, R. T. (2015). Oceanic forcing of ice-sheet retreat: West Antarctica and more. *Annual Review of Earth and Planetary Sciences*, *43*(1), 207-231. Retrieved from `https://doi.org/10.1146/annurev-earth-060614-105344` doi: 10.1146/annurev-earth-060614-105344

Bamber, J. L. (2000). *Antarctic 5-km digital elevation model from ERS-1 altimetry, version 1.* NASA National Snow and Ice Data Center Distributed Active Archive Center, Boulder, Colorado USA. Retrieved from `https://doi.org/10.5067/BZVCEDZWUTCH` (Accessed: 2020-07-28)

Bamber, J. L., Riva, R. E. M., Vermeersen, B. L. A., & LeBrocq, A. M. (2009). Reassessment of the potential sea-level rise from a collapse of the West Antarctic Ice Sheet. *Science*, *324*(5929), 901-903. Retrieved from `http://science.sciencemag.org/content/324/5929/901` doi: 10.1126/science.1169335

Barnes, J. M., Dias dos Santos, T., Goldberg, D., Gudmundsson, G. H., Morlighem, M., & De Rydt, J. (2021). The transferability of adjoint inversion products between different ice flow models. *The Cryosphere*, *15*(4), 1975–2000. Retrieved from `https://tc.copernicus.org/articles/15/1975/2021/` doi: 10.5194/tc-15-1975-2021

Blatter, H. (1995). Velocity and stress-fields in grounded glaciers: A simple algorithm for including deviatoric stress gradients. *J Glaciol*, *41*(138), 333-344.

Brondex, J., Gagliardini, O., Gillet-Chaulet, F., & Durand, G. (2017). Sensitivity of grounding line dynamics to the choice of the friction law. *Journal of Glaciology*, *63*(241), 854–866. doi: 10.1017/jog.2017.51

Brondex, J., Gillet-Chaulet, F., & Gagliardini, O. (2019). Sensitivity of centennial mass loss projections of the Amundsen basin to the friction law. *The Cryosphere*, *13*(1), 177-195. Retrieved from `https://www.the-cryosphere.net/13/177/2019/` doi: 10.5194/tc-13-177-2019

Burton, J. C., Amundson, J. M., Cassotto, R., Kuo, C.-C., & Dennin, M. (2018). Quantifying flow and stress in ice mélange, the world's largest granular material. *Proceedings of the National Academy of Sciences*, *115*(20), 5105–5110. Retrieved from `https://www.pnas.org/content/115/20/5105` doi: 10.1073/pnas.1715136115

Cornford, S. L., Seroussi, H., Asay-Davis, X. S., Gudmundsson, G. H., Arthern, R., Borstad, C., ... Yu, H. (2020). Results of the third Marine Ice Sheet Model Intercomparison Project (MISMIP+). *The Cryosphere*, *14*(7), 2283–2301. Retrieved from `https://tc.copernicus.org/articles/14/2283/2020/` doi: 10.5194/tc-14-2283-2020

Crawford, A. J., Benn, D. I., Todd, J., Åström, J. A., Bassis, J. N., & Zwinger, T.

(2021, May 11). Marine ice-cliff instability modeling shows mixed-mode ice-cliff failure and yields calving rate parameterization. *Nature Communications*, *12*(1), 2701. Retrieved from https://doi.org/10.1038/s41467-021-23070-7 doi: 10.1038/s41467-021-23070-7

Depoorter, M. A., Bamber, J. L., Griggs, J. A., Lenaerts, J. T. M., Ligtenberg, S. R. M., van den Broeke, M. R., & Moholdt, G. (2013, Oct 01). Calving fluxes and basal melt rates of Antarctic ice shelves. *Nature*, *502*(7469), 89-92. Retrieved from https://doi.org/10.1038/nature12567 doi: 10.1038/nature12567

De Rydt, J., Reese, R., Paolo, F. S., & Gudmundsson, G. H. (2021). Drivers of Pine Island Glacier speed-up between 1996 and 2016. *The Cryosphere*, *15*(1), 113–132. Retrieved from https://tc.copernicus.org/articles/15/113/2021/ doi: 10.5194/tc-15-113-2021

Durand, G., Gagliardini, O., Favier, L., Zwinger, T., & Le Meur, E. (2011). Impact of bedrock description on modeling ice sheet dynamics. *Geophysical Research Letters*, *38*(20), 1-6. Retrieved from https://agupubs.onlinelibrary.wiley.com/doi/abs/10.1029/2011GL048892 doi: 10.1029/2011GL048892

Favier, L., Durand, G., Cornford, S. L., Gudmundsson, G. H., Gagliardini, O., Gillet-Chaulet, F., … Le Brocq, A. M. (2014). Retreat of Pine Island Glacier controlled by marine ice-sheet instability. *Nature Climate Change*, *4*, 117-121. Retrieved from https://www.nature.com/articles/nclimate2094#supplementary-information doi: 10.1038/nclimate2094

Feldmann, J., & Levermann, A. (2015). Collapse of the West Antarctic Ice Sheet after local destabilization of the Amundsen Basin. *Proceedings of the National Academy of Sciences*, *112*(46), 14191-14196. Retrieved from http://www.pnas.org/content/112/46/14191 doi: 10.1073/pnas.1512482112

Fretwell, P., Pritchard, H. D., Vaughan, D. G., Bamber, J. L., Barrand, N. E., Bell, R., … Zirizzotti, A. (2013). Bedmap2: improved ice bed, surface and thickness datasets for Antarctica. *The Cryosphere*, *7*(1), 375-393. Retrieved from https://www.the-cryosphere.net/7/375/2013/ doi: 10.5194/tc-7-375-2013

Goldberg, D. N. (2011). A variationally derived, depth-integrated approximation to a higher-order glaciological flow model. *Journal of Glaciology*, *57*(201), 157–170. doi: 10.3189/002214311795306763

Goldberg, D. N., & Heimbach, P. (2013). Parameter and state estimation with a time-dependent adjoint marine ice sheet model. *The Cryosphere*, *7*(6), 1659–1678. Retrieved from https://tc.copernicus.org/articles/8/1659/2013/ doi: 10.5194/tc-7-1659-2013

Gudmundsson, G. H. (2020). *GHilmarG/UaSource: Ua2019b (version v2019b).* Zenodo. Retrieved from http://doi.org/10.5281/zenodo.3706623

Gudmundsson, G. H., Krug, J., Durand, G., Favier, L., & Gagliardini, O. (2012). The stability of grounding lines on retrograde slopes. *The Cryosphere*, *6*(6), 1497-1505. Retrieved from https://www.the-cryosphere.net/6/1497/2012/ doi: 10.5194/tc-6-1497-2012

Gudmundsson, G. H., Paolo, F. S., Adusumilli, S., & Fricker, H. A. (2019). Instantaneous Antarctic ice sheet mass loss driven by thinning ice shelves. *Geophys Res Lett*, *46*(23), 13903-13909. Retrieved from https://agupubs.onlinelibrary.wiley.com/doi/abs/10.1029/2019GL085027 doi: 10.1029/2019GL085027

Hoffman, M. J., Asay-Davis, X., Price, S. F., Fyke, J., & Perego, M. (2019). Effect of subshelf melt variability on sea level rise contribution from Thwaites Glacier, Antarctica. *Journal of Geophysical Research: Earth Surface*, *124*(12), e2019JF005155. Retrieved from https://agupubs.onlinelibrary.wiley.com/doi/abs/10.1029/2019JF005155 (e2019JF005155 10.1029/2019JF005155) doi: 10.1029/2019JF005155

Hogan, K. A., Larter, R. D., Graham, A. G. C., Arthern, R., Kirkham, J. D., Totten Minzoni, R., … Wellner, J. (2020). Revealing the former bed of Thwaites Glacier using sea-floor bathymetry: implications for warm-water routing and bed controls on ice flow and buttressing. *The Cryosphere*, *14*(9), 2883–2908. Retrieved from https://tc.copernicus.org/articles/14/2883/2020/ doi: 10.5194/tc-14-2883-2020

Holt, J. W., Blankenship, D. D., Morse, D. L., Young, D. A., Peters, M. E., Kempf, S. D., … Corr, H. F. J. (2006). New boundary conditions for the West Antarctic Ice Sheet: Subglacial topography of the Thwaites and Smith glacier catchments. *Geophysical Research Letters*, *33*(9). Retrieved from https://agupubs.onlinelibrary.wiley.com/doi/abs/10.1029/2005GL025561 doi: 10.1029/2005GL025561

Howat, I. M., Porter, C., Smith, B. E., Noh, M.-J., & Morin, P. (2019). The reference elevation model of Antarctica. *The Cryosphere*, *13*(2), 665–674. Retrieved from https://www.the-cryosphere.net/13/665/2019/ doi: 10.5194/tc-13-665-2019

Jenkins, A., Dutrieux, P., Jacobs, S., Steig, E. J., Gudmundsson, G. H., Smith, J., & Heywood, K. J. (2016, December). Decadal ocean forcing and Antarctic Ice Sheet response: Lessons from the Amundsen Sea. *Oceanography*, *29*(4), 106-117. Retrieved from https://doi.org/10.5670/oceanog.2016.103

Jordan, T. A., Porter, D., Tinto, K., Millan, R., Muto, A., Hogan, K., … Paden, J. D. (2020). New gravity-derived bathymetry for the Thwaites, Crosson, and Dotson ice shelves revealing two ice shelf populations. *The Cryosphere*, *14*(9), 2869–2882. Retrieved from https://tc.copernicus.org/articles/14/2869/2020/ doi: 10.5194/tc-14-2869-2020

Joughin, I., Smith, B. E., & Medley, B. (2014). Marine ice sheet collapse potentially under way for the Thwaites Glacier Basin, West Antarctica. *Science*, *344*(6185), 735-738. Retrieved from http://science.sciencemag.org/content/344/6185/735 doi: 10.1126/science.1249055

Joughin, I., Smith, B. E., & Schoof, C. G. (2019). Regularized Coulomb friction laws for ice sheet sliding: Application to Pine Island Glacier, Antarctica. *Geophysical Research Letters*, *46*(9), 4764-4771. Retrieved from https://agupubs.onlinelibrary.wiley.com/doi/abs/10.1029/2019GL082526 doi: 10.1029/2019GL082526

Konrad, H., Shepherd, A., Gilbert, L., Hogg, A. E., McMillan, M., Muir, A., & Slater, T. (2018). Net retreat of Antarctic glacier grounding lines. *Nature Geoscience*, *11*, 258-262. Retrieved from https://doi.org/10.1038/s41561-018-0082-z doi: 10.1038/s41561-018-0082-z

Larour, E., Seroussi, H., Morlighem, M., & Rignot, E. (2012). Continental scale, high order, high spatial resolution, ice sheet modeling using the Ice Sheet System Model (ISSM). *J Geophys Res Earth Surf*, *117*(F1), 1-20. Retrieved from https://agupubs.onlinelibrary.wiley.com/doi/abs/10.1029/2011JF002140 doi: 10.1029/2011JF002140

Lipscomb, W. H., Price, S. F., Hoffman, M. J., Leguy, G. R., Bennett, A. R., Bradley, S. L., … Worley, P. H. (2019). Description and evaluation of the Community Ice Sheet Model (CISM) v2.1. *Geoscientific Model Development*, *12*(1), 387–424. Retrieved from https://www.geosci-model-dev.net/12/387/2019/ doi: 10.5194/gmd-12-387-2019

MacAyeal, D. (1989). Large-scale ice flow over a viscous basal sediment: Theory and application to ice stream B, Antarctica. *Journal of Geophysical Research: Solid Earth*, *94*(B4), 4071-4087. Retrieved from https://agupubs.onlinelibrary.wiley.com/doi/abs/10.1029/JB094iB04p04071 doi: 10.1029/JB094iB04p04071

MacGregor, J. A., Catania, G. A., Markowski, M. S., & Andrews, A. G. (2012). Widespread rifting and retreat of ice-shelf margins in the eastern Amundsen Sea Embayment between 1972 and 2011. *Journal of Glaciology*, *58*(209),

458–466. doi: 10.3189/2012JoG11J262
Martin, D. F., Cornford, S. L., & Payne, A. J. (2019). Millennial-scale vulnerability of the Antarctic Ice Sheet to regional ice shelf collapse. *Geophysical Research Letters*, *46*(3), 1467-1475. Retrieved from `https://agupubs.onlinelibrary.wiley.com/doi/abs/10.1029/2018GL081229` doi: 10.1029/2018GL081229
Miles, B. W. J., Stokes, C. R., Jenkins, A., Jordan, J. R., Jamieson, S. S. R., & Gudmundsson, G. H. (2020). Intermittent structural weakening and acceleration of the Thwaites Glacier Tongue between 2000 and 2018. *Journal of Glaciology*, *66*(257), 485–495. doi: 10.1017/jog.2020.20
Milillo, P., Rignot, E., Rizzoli, P., Scheuchl, B., Mouginot, J., Bueso-Bello, J., & Prats-Iraola, P. (2019). Heterogeneous retreat and ice melt of Thwaites Glacier, West Antarctica. *Science Advances*, *5*(1). Retrieved from `http://advances.sciencemag.org/content/5/1/eaau3433` doi: 10.1126/sciadv.aau3433
Morlighem, M., Rignot, E., Binder, T., Blankenship, D., Drews, R., Eagles, G., ... Young, D. A. (2020, Feb 01). Deep glacial troughs and stabilizing ridges unveiled beneath the margins of the Antarctic ice sheet. *Nature Geoscience*, *13*(2), 132-137. Retrieved from `https://doi.org/10.1038/s41561-019-0510-8` doi: 10.1038/s41561-019-0510-8
Mouginot, J., Rignot, E., & Scheuchl, B. (2014). Sustained increase in ice discharge from the Amundsen Sea Embayment, West Antarctica, from 1973 to 2013. *Geophysical Research Letters*, *41*(5), 1576-1584. Retrieved from `https://agupubs.onlinelibrary.wiley.com/doi/abs/10.1002/2013GL059069` doi: 10.1002/2013GL059069
Nakayama, Y., Manucharyan, G., Zhang, H., Dutrieux, P., Torres, H. S., Klein, P., ... Menemenlis, D. (2019, Nov 22). Pathways of ocean heat towards Pine Island and Thwaites grounding lines. *Scientific Reports*, *9*(1), 16649. Retrieved from `https://doi.org/10.1038/s41598-019-53190-6` doi: 10.1038/s41598-019-53190-6
Nakayama, Y., Menemenlis, D., Zhang, H., Schodlok, M., & Rignot, E. (2018, Aug 24). Origin of Circumpolar Deep Water intruding onto the Amundsen and Bellingshausen Sea continental shelves. *Nature Communications*, *9*(1), 3403. Retrieved from `https://doi.org/10.1038/s41467-018-05813-1` doi: 10.1038/s41467-018-05813-1
Nias, I. J., Cornford, S. L., & Payne, A. J. (2016). Contrasting the modelled sensitivity of the Amundsen Sea Embayment ice streams. *Journal of Glaciology*, *62*(233), 552–562. doi: 10.1017/jog.2016.40
Paolo, F. S., Fricker, H. A., & Padman, L. (2015). Volume loss from Antarctic ice shelves is accelerating. *Science*, *348*(6232), 327-331. Retrieved from `http://science.sciencemag.org/content/348/6232/327` doi: 10.1126/science.aaa0940
Pritchard, H. D., Ligtenberg, S. R. M., Fricker, H. A., Vaughan, D. G., van den Broeke, M. R., & Padman, L. (2012, Apr 01). Antarctic ice-sheet loss driven by basal melting of ice shelves. *Nature*, *484*(7395), 502-505. Retrieved from `https://doi.org/10.1038/nature10968` doi: 10.1038/nature10968
Rignot, E., Jacobs, S., Mouginot, J., & Scheuchl, B. (2013). Ice-shelf melting around Antarctica. *Science*, *341*(6143), 266–270. Retrieved from `https://science.sciencemag.org/content/341/6143/266` doi: 10.1126/science.1235798
Rignot, E., Mouginot, J., Morlighem, M., Seroussi, H., & Scheuchl, B. (2014). Widespread, rapid grounding line retreat of Pine Island, Thwaites, Smith, and Kohler glaciers, West Antarctica, from 1992 to 2011. *Geophysical Research Letters*, *41*(10), 3502-3509. Retrieved from `https://agupubs.onlinelibrary.wiley.com/doi/abs/10.1002/2014GL060140` doi: 10.1002/2014GL060140
Robel, A. A., Seroussi, H., & Roe, G. H. (2019). Marine ice sheet instability amplifies and skews uncertainty in projections of future sea-level rise.

Proceedings of the National Academy of Sciences, *116*(30), 14887–14892. Retrieved from https://www.pnas.org/content/116/30/14887 doi: 10.1073/pnas.1904822116

Scambos, T., Bell, R., Alley, R., Anandakrishnan, S., Bromwich, D., Brunt, K., … Yager, P. (2017). How much, how fast?: A science review and outlook for research on the instability of Antarctica's Thwaites Glacier in the 21st century. *Global and Planetary Change*, *153*, 16 - 34. Retrieved from http://www.sciencedirect.com/science/article/pii/S092181811630491X doi: https://doi.org/10.1016/j.gloplacha.2017.04.008

Scambos, T., Fricker, H. A., Liu, C.-C., B., J., Fastook, J., Sargent, A., … Wu, A.-M. (2009). Ice shelf disintegration by plate bending and hydro-fracture: Satellite observations and model results of the 2008 Wilkins ice shelf breakups. *Earth and Planetary Science Letters*, *280*(1), 51-60. Retrieved from http://www.sciencedirect.com/science/article/pii/S0012821X08007887 doi: https://doi.org/10.1016/j.epsl.2008.12.027

Schoof, C. (2007). Ice sheet grounding line dynamics: Steady states, stability, and hysteresis. *Journal of Geophysical Research: Earth Surface*, *112*(F3), 1-19. Retrieved from https://agupubs.onlinelibrary.wiley.com/doi/abs/10.1029/2006JF000664 doi: 10.1029/2006JF000664

Seroussi, H., & Morlighem, M. (2018). Representation of basal melting at the grounding line in ice flow models. *The Cryosphere*, *12*(10), 3085-3096. Retrieved from https://www.the-cryosphere.net/12/3085/2018/ doi: 10.5194/tc-12-3085-2018

Seroussi, H., Morlighem, M., Larour, E., Rignot, E., & Khazendar, A. (2014). Hydrostatic grounding line parameterization in ice sheet models. *The Cryosphere*, *8*(6), 2075-2087. Retrieved from https://www.the-cryosphere.net/8/2075/2014/ doi: 10.5194/tc-8-2075-2014

Seroussi, H., Nakayama, Y., Larour, E., Menemenlis, D., Morlighem, M., Rignot, E., & Khazendar, A. (2017). Continued retreat of Thwaites Glacier, West Antarctica, controlled by bed topography and ocean circulation. *Geophysical Research Letters*, *44*(12), 6191-6199. Retrieved from https://agupubs.onlinelibrary.wiley.com/doi/abs/10.1002/2017GL072910 doi: 10.1002/2017GL072910

Seroussi, H., Nowicki, S., Payne, A. J., Goelzer, H., Lipscomb, W. H., Abe-Ouchi, A., … Zwinger, T. (2020). ISMIP6 Antarctica: a multi-model ensemble of the Antarctic ice sheet evolution over the 21st century. *The Cryosphere*, *14*(9), 3033–3070. Retrieved from https://tc.copernicus.org/articles/14/3033/2020/ doi: 10.5194/tc-14-3033-2020

Seroussi, H., Nowicki, S., Simon, E., Abe-Ouchi, A., Albrecht, T., Brondex, J., … Zhang, T. (2019). initMIP-Antarctica: an ice sheet model initialization experiment of ISMIP6. *The Cryosphere*, *13*(5), 1441–1471. Retrieved from https://tc.copernicus.org/articles/13/1441/2019/ doi: 10.5194/tc-13-1441-2019

Shepherd, A., Gilbert, L., Muir, A. S., Konrad, H., McMillan, M., Slater, T., … Engdahl, M. E. (2019). Trends in Antarctic Ice Sheet elevation and mass. *Geophysical Research Letters*, *46*(14), 8174-8183. Retrieved from https://agupubs.onlinelibrary.wiley.com/doi/abs/10.1029/2019GL082182 doi: 10.1029/2019GL082182

Smith, B., Fricker, H. A., Gardner, A. S., Medley, B., Nilsson, J., Paolo, F. S., … Zwally, H. J. (2020). Pervasive ice sheet mass loss reflects competing ocean and atmosphere processes. *Science*, *368*(6496), 1239–1242. Retrieved from https://science.sciencemag.org/content/368/6496/1239 doi: 10.1126/science.aaz5845

Van Liefferinge, B., & Pattyn, F. (2013). Using ice-flow models to evaluate potential sites of million year-old ice in Antarctica. *Climate of the Past*, *9*(5), 2335–

2345. Retrieved from https://cp.copernicus.org/articles/9/2335/2013/ doi: 10.5194/cp-9-2335-2013

Van Wessem, J., Reijmer, C., Morlighem, M., Mouginot, J., Rignot, E., Medley, B., ... Van Meijgaard, E. (2014). Improved representation of East Antarctic surface mass balance in a regional atmospheric climate model. *Journal of Glaciology*, *60*(222), 761–770. doi: 10.3189/2014JoG14J051

Weertman, J. (1957). On the sliding of glaciers. *Journal of Glaciology*, *3*(21), 33–38. doi: 10.3189/S0022143000024709

Weertman, J. (1974). Stability of the junction of an ice sheet and an ice shelf. *Journal of Glaciology*, *13*(67), 3-11. doi: 10.3189/S0022143000023327

Figure 1.

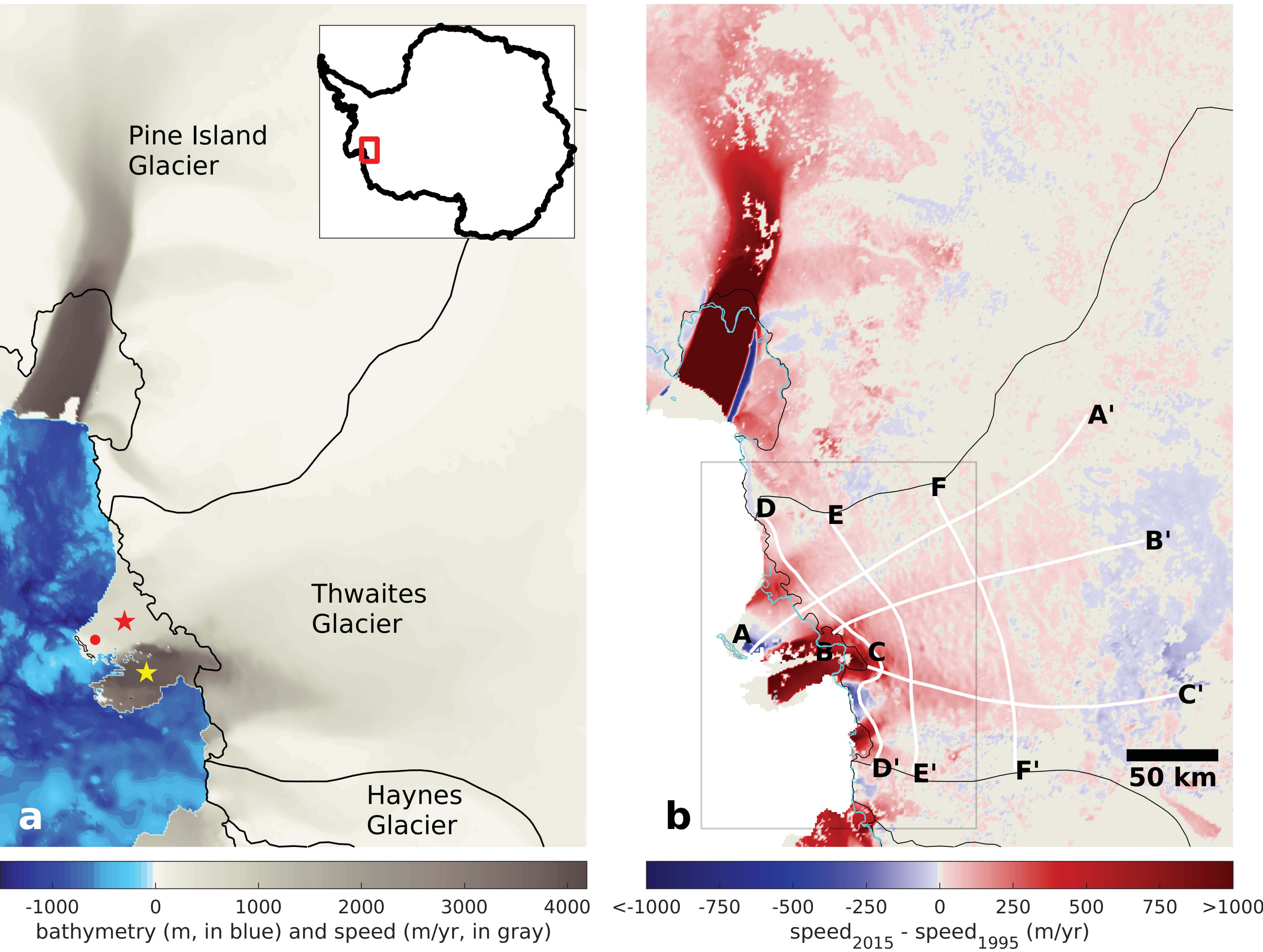
Pine Island Glacier
Thwaites Glacier
Haynes Glacier
a
-1000
0
1000
2000
3000
4000
bathymetry (m, in blue) and speed (m/yr, in gray)
A'
B'
C'
D
E
F
A
B
C
D'
E'
F'
50 km
b
<-1000
-750
-500
-250
0
250
500
750
>1000
speed2015 - speed1995 (m/yr)

Figure 2.

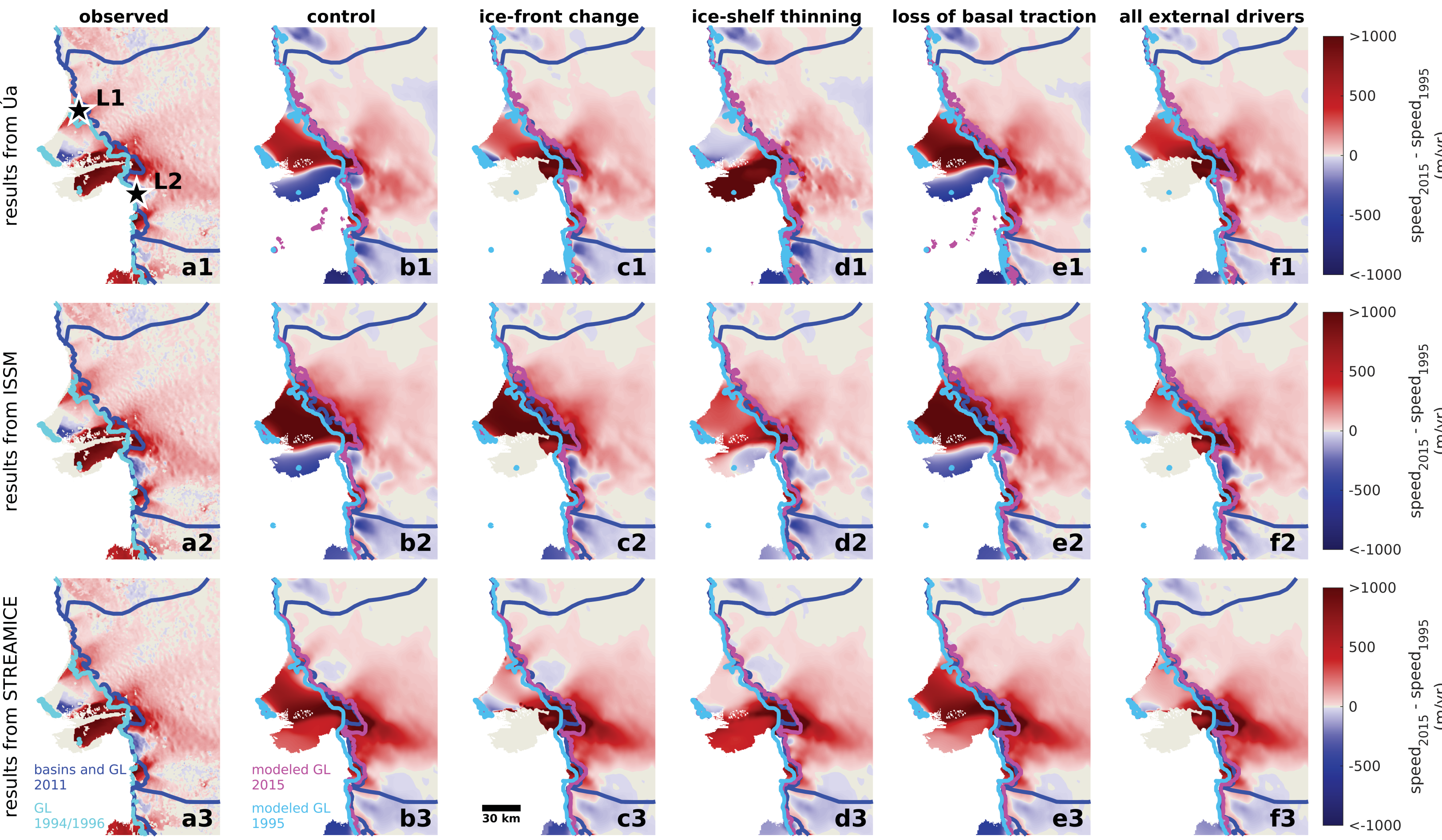
observed
control
ice-front change
ice-shelf thinning
loss of basal traction
all external drivers
results from Úa
results from ISSM
results from STREAMICE
L1
L2
a1
b1
c1
d1
e1
f1
a2
b2
c2
d2
e2
f2
a3
b3
c3
d3
e3
f3
basins and GL 2011
GL 1994/1996
modeled GL 2015
modeled GL 1995
30 km
>1000
500
0
-500
<-1000
speed$_{2015}$ - speed$_{1995}$ (m/yr)

Figure 3.

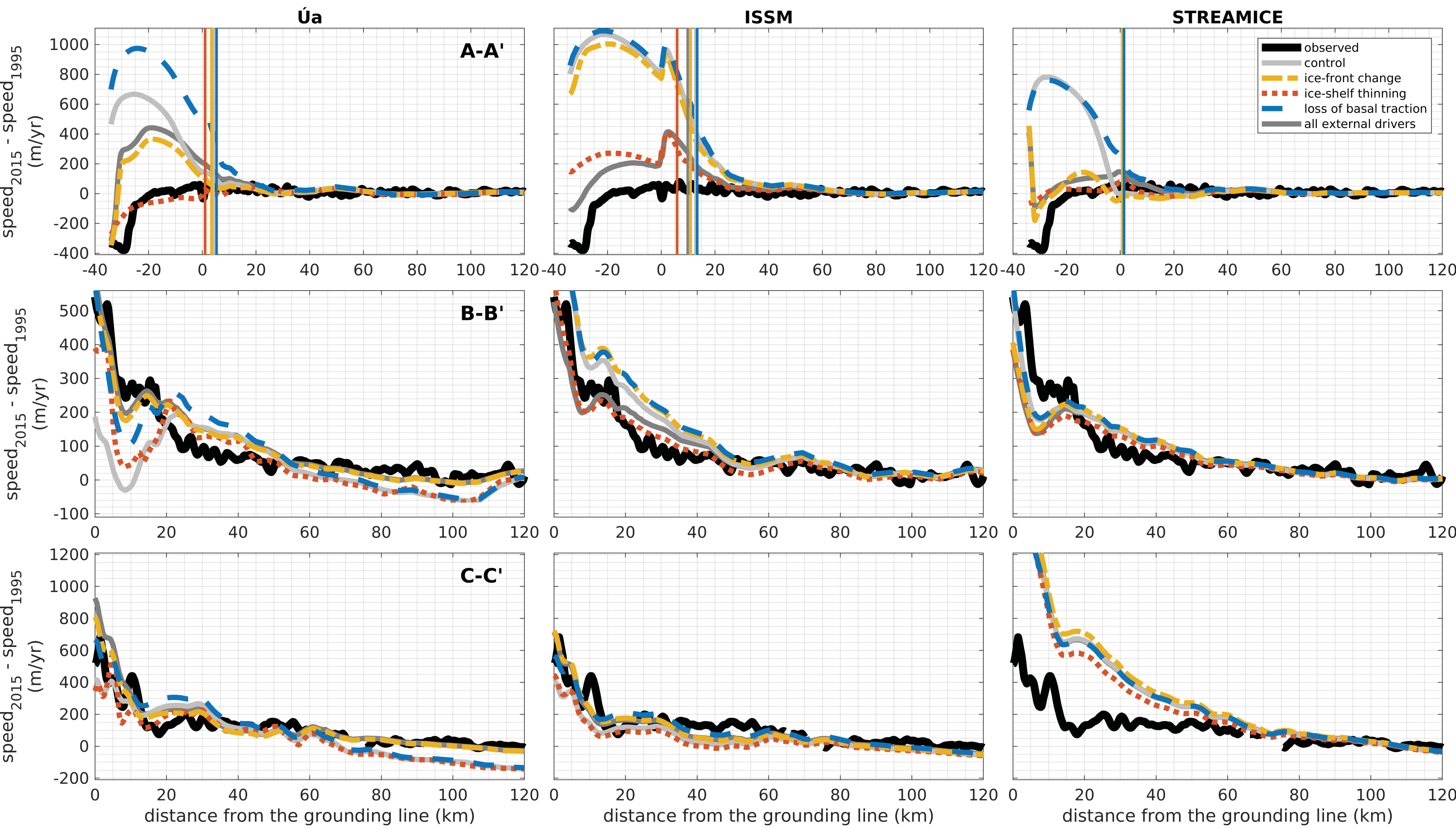
Úa
ISSM
STREAMICE
A-A'
B-B'
C-C'
observed
control
ice-front change
ice-shelf thinning
loss of basal traction
all external drivers
speed2015 - speed1995 (m/yr)
distance from the grounding line (km)